Surface conductivity of insulators: a resistivity measurement technique under vacuum

Surface conductivity of insulators: a resistivity measurement technique under vacuum

A H Soliman, S R Holcombe, P J Pigram and J Liesegang[1]

Department of Physics, La Trobe University, Melbourne, VIC 3086, Australia

E-mail: J.Liesegang@latrobe.edu.au

Abstract
A method of resistivity measurement for insulators, previously described by
Liesegang and Senn (1995 *J. Appl. Phys.* **77** 5782; 1996 *J. Appl. Phys.* **80** 6336),
has been demonstrated to produce measurements not only in good agreement
with established results in the literature but also with improved accuracy. The
method is based on monitoring the discharge of a charged sample of an insulator
through a grounded boundary. The measurements, however, were performed
under atmospheric conditions and so the results were influenced by atmospheric
effects such as temperature and moisture. By confining a sample to a vacuum
and charging it via a custom built electron gun, we here extend the established
method of Liesegang and Senn to a more controlled environment. In this
paper, we numerically solve the potential and transport equations for the axial–
cylindrical geometry of the system and present comparisons of theory and
experiment through derived values of the resistivity, carrier depth and diffusion
constant for a range of insulator samples. We also use asymptotic solutions via
a theory of Burgers equation shock waves, as discussed in Holcombe *et al* (2004
J. Phys. Condens. Matter **16** 5999), to derive resistivity values and again draw
comparisons. The results presented here are also compared with previously
obtained or literature measurements of resistivity.

1. Introduction

It is of increasing importance to be able to specify accurately the resistivity of insulating
materials, particularly as may apply in their surface regions. By way of illustration, some
published values of resistivity for polyethylene from various literature sources are 10^{13}–
10^{16} [1], 10^{14} [2] and 10^{18} Ω m [3, 4]. It is believed that the notably large disparity in these
reported measurements is due to the common methodology of attaching electrical contacts
for the application of known potential and consequent measurement of current flow. It is not

---

[1] Author to whom any correspondence should be addressed.

uncommon, it would seem, for contact resistance to play an unintended role in the resistivity measurement of insulator samples.

In 1995, Liesegang and Senn [5] devised a method for resistivity measurement of insulators which avoided these contact problems, and which is based on the decay of charge from a charged insulator surface through a grounded boundary edge. The method enables determination of resistivity with typical accuracy of about $\pm 10\%$ and is akin to that described in the 'Annual Book of ASTM Standards' [6], except that the latter gives an interpretation which is erroneous in that it claims the charge decay to be exponential with time. This point has been discussed at length in [5].

Further to approximations which were made in [5], later [7, 8] provided a more accurate description of the processes of charge decay from samples, resulting in improved resistivity measurement. These were nevertheless still based on a Cartesian geometry and related to experiments performed under atmospheric conditions.

The purpose of the present paper is to reformulate the above description in terms of the new cylindrical geometry incorporated in a newly constructed vacuum system for resistivity measurement as well as to report on deductions to be drawn from new developments of charge transport in the surface regions of insulators [9], from which additional insight may be drawn regarding the resistivity determinations.

2. Experimental configuration

The vacuum resistivity system comprises: a high vacuum chamber incorporating two manipulators, a custom designed electron gun, a digital electrometer (Keithley Model 6517), a custom data acquisition program created using TestPoint® software to control the system. The measurement technique is similar in principle to that defined in [5–8]; however, the vacuum environment reduces the probability of contamination and allows greater control of the nature of the surface of the sample.

The chamber is of axially symmetric cylindrical construction, 263 mm in diameter and 268 mm in height (figure 1.1). It is electrically grounded and pumped with rotary and turbomolecular (Leybold-Heraeus) pumps. The working pressure inside the chamber during experimental work is about 10^{-7}–10^{-8} hPa. The chamber has six standard (70 mm flanges) on short tubulations perpendicular to the side of the chamber and near to the top edge of the chamber. These ports are utilized by the following: (a) an ultrahigh vacuum ionization gauge (Granville-Philips), (b) a 12-pin feedthrough utilized to connect the applied voltages to the electrodes inside the chamber, (c) nitrogen venting to facilitate rapid pumpdown, (d) a horizontal manipulator and (e) window flanges. The top flange of the chamber supports a second manipulator (vertical). The vertical and horizontal manipulators are respectively used to translate the sample and to position an adjacent mesh which acts as a capacitive electrode.

The sample is sandwiched between two circular stainless steel pieces (see figure 1.2). The bottom piece is annular with inside and outside diameters of 10 and 26 mm, respectively. This sample holder is suspended from a vertical stainless steel cylindrical bar of length 221 mm. The bar and the sample holder are isolated from each other by a spacer of Teflon of length 65 mm. The bar was mounted on the standard flange (70 mm), which is equipped with a connector for voltage connection outside the chamber.

With the sample confined in a vacuum chamber, frictional charging methods employed in [1] are replaced by secondary-electron emission using a custom designed electron gun. The electron gun comprises: (a) a tungsten filament coupled to a power supply (20 V; 30 A), (b) four electrodes of different geometries and applied voltages for focusing electrons onto the sample area. Details about the geometries and the applied voltages for each electrode of the electron
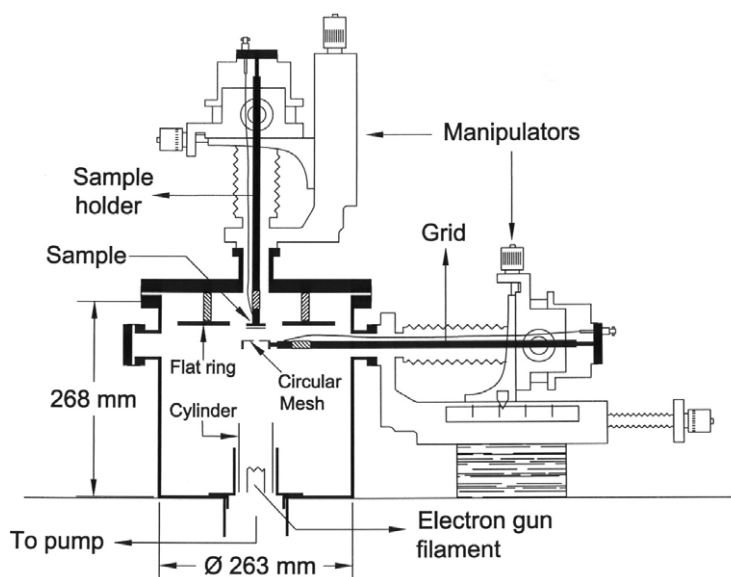
Figure 1.1. An axial cross-sectional elevation drawing showing the vacuum chamber, manipulators, the sample, the electron gun and the capacitively coupled mesh electrode which was connected to an electrometer.
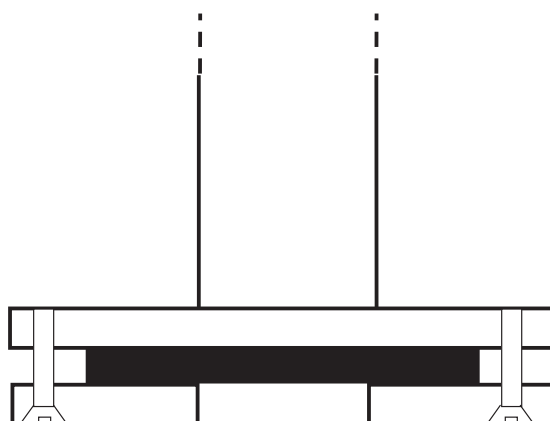

Figure 1.2. A schematic more detailed cross-sectional drawing of the sample (shaded black) holder, showing a typical sample sandwiched between two circular metal plates. The exposed circular surface of the sample is about 10 mm in diameter and its edge is electrically grounded via the bottom plate and the supporting rod shown, which is attached to the vertical manipulator atop the chamber.

gun are: (i) a circular electrode, which holds the sample (500 V), (ii) a circular flat ring of inside and outside diameters 60 and 130 mm with applied voltage 1000 V—this ring is affixed to the top of the chamber by three insulating rods (35 mm length) made from ceramic material, (iii) a circular mesh (at 480 V), capacitively coupled below the sample and connected to an electrometer for recording the charge decay and (iv) a cylindrical electron gun lens electrode (−1 V); see figure 1.3. The figure also shows the simulation of electron trajectories, performed using the SIMION 3D computer program.
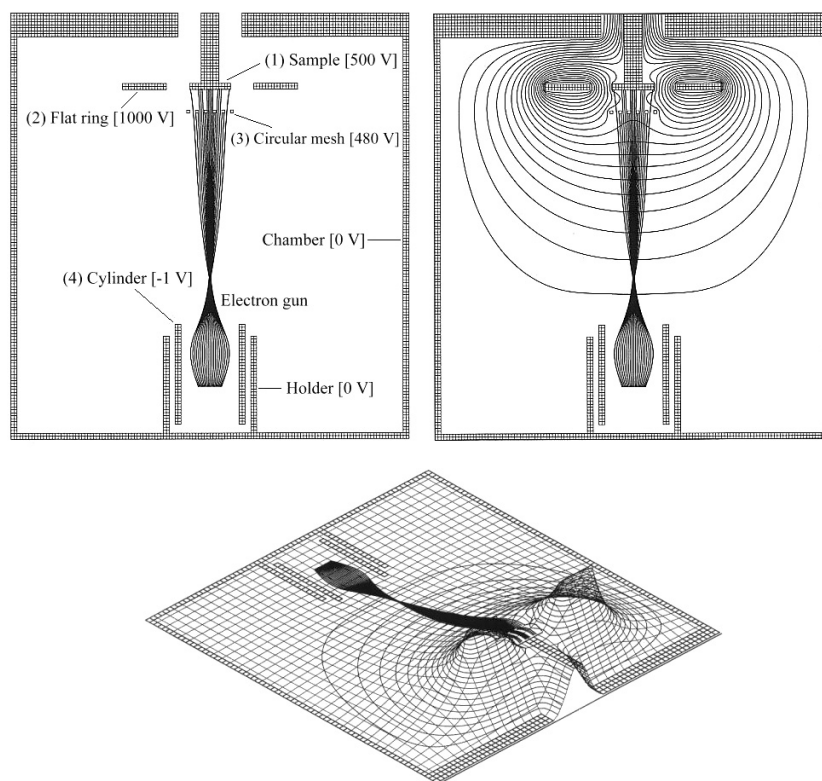
Figure 1.3. Simulation of the electron lens trajectories performed with the SIMION 3D computer program. Above left are shown the electrode designations and voltages used during the secondary emission/sample charging process. Above right is shown a plot of equipotential curves and below is shown a similar 3D representation of the potential contours. All three diagrams show a defocused electron beam striking the exposed 10 mm diameter sample.

A data acquisition and control package was created using TestPoint® program software from Capital Equipment Corporation, USA. It provides combined hardware/software for transferring the charge (electrometer voltage) decay data directly from the digital electrometer (Keithley Model 6517) to a PC.

2.1. Experimental procedure

Samples were first mounted into the sample holder, and the system pumped to a working pressure of 10^{-7}–10^{-8} hPa. Voltages were applied to the four electrodes inside the vacuum chamber to allow the sample to be charged by secondary-electron emission using a broadly focused beam of incident electrons. The electrodes were then disconnected manually and the mesh electrode grounded and connected to the digital electrometer. Finally the sample was grounded and the charge decay monitored. Charge decay data were then transferred into a PC through the data acquisition control software and saved in file for later analysis. These steps were performed manually; charge decay from insulators is slow.

An initial test was carried out to verify the relation between the electric potential for the initial charge decay V_0 (volts) versus $1/d$ (mm^{-1}) and the charge Q_0 (coulombs) versus d (mm), where d is the distance between the sample and the grid. Using the procedure above,
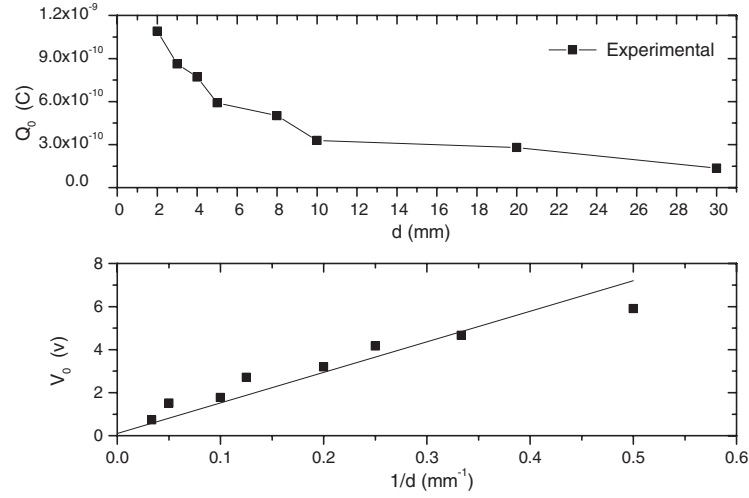
Figure 2.1. The initial (immediately after charging the sample) mesh electric potential V_0 (volts) and the initial charge Q_0 (coulombs) as a function of $1/d$ and d (mm), respectively, for a glass sample (d is the distance between the sample and the mesh).

initial voltages were obtained at different d values. Figure 2.1 shows these relations for a glass sample. As expected, the field strength is inversely proportional to the distance from the charged sample, which provides a good indication of the validity of the results obtained from the system.

3. Charge transport in cylindrical coordinates

We first note that our system of charge transport is governed by the following set of coupled partial differential equations that are not dependent on an angular term due to the symmetry of the system [3, 9]:

$$\frac{1}{r}\frac{\partial}{\partial r}\left(r\frac{\partial\phi}{\partial r}\right) + \frac{\partial^2\phi}{\partial z^2} = -an(r,t) \qquad r < R_s, \quad z = H_s \quad \text{Poisson's equation} \tag{3.1}$$

$$\frac{\partial n}{\partial t} = \beta\left(\frac{\partial\phi}{\partial r}\frac{\partial n}{\partial r} - \alpha n^2\right) \qquad r < R_s, \quad z = H_s \tag{3.2}$$

$$\frac{1}{r}\frac{\partial}{\partial r}\left(r\frac{\partial\phi}{\partial r}\right) + \frac{\partial^2\phi}{\partial z^2} = 0 \qquad \forall r, \quad z/\{z = H_s\} \quad \text{Laplace's equation.} \tag{3.3}$$

Poisson's equation (3.1) holds in the domain of the charged sample surface. Laplace's equation holds in the remainder of the chamber space. Equation (3.2) for the charge carrier density is derived in the domain of the sample by combining equation (3.1) with Ohm's law and the equation of continuity [3, 5, 7].

Here the radial coordinate r is measured from the axis of the chamber or sample and $\phi(r, z)$ is the potential function; $n(r, t)$ is the charge carrier density in the surface region of the sample; $\alpha = q/\varepsilon\varepsilon_0$ and $\beta = qD/kT$, where D is the carrier diffusion constant [3]. We have defined R_s and H_s to be the radius and height of the sample in the chamber respectively, where we take H_s to be the length measured from the base of the chamber taken to be $z = 0$. Further to this we define the radius and height of the chamber as R_c and H_c, respectively, where the height is defined to be that taken from the base at $z = 0$ to its full height at $z = H_c$.

The following boundary and initial conditions for the potential describe both the grounding of the chamber and the outer edge of the sample ($r = R_s$):

$$\phi(R_s, H_s) = 0$$
$$\phi(R_c, z) = 0$$
$$\phi(r, H_c) = 0$$
$$\phi(r, 0) = 0. \tag{3.4}$$

The initial ($t = 0$) charge carrier density $n(r, t)$ in the surface region of the sample is taken for simplicity to be uniform or constant:

$$n(r, 0) = n_0. \tag{3.5}$$

We now note that due to the angular symmetry of the system we essentially have a numerical scheme appropriate to a two-dimensional plane (r, z) and also note that in (3.1) and (3.3) we have a singularity at $r = 0$, so this must be treated as a particular case in the final numerical implementation.

This 2D sheet in computation may be visualized as a rectangle that has its leftmost boundary (i.e. $r = 0$) as the axis of symmetry and thus we must have

$$\frac{\partial \phi(0, z)}{\partial r} = 0, \qquad \frac{\partial n(0, t)}{\partial r} = 0. \tag{3.6}$$

Also in this 2D sheet, we will have a line starting from the leftmost boundary and finishing at $r = R_s$, at a height of $z = H_s$, representing the sample. With this configuration and the dependence of the differential equations on the domain of relaxation, we note there are four main areas that will require separate finite difference representation for the purposes of calculating the potential. The first is that of the actual sample, in which we have (3.1), defining the potential due to a surface charge carrier density. We may use a central finite difference scheme for (3.1) excluding $r = 0$, for $t = 0$:

$$\frac{\phi_{j+1,i}^k - 2\phi_{j,i}^k + \phi_{j-1,i}^k}{\Delta r^2} + \frac{\phi_{j,i+1}^k - 2\phi_{j,i}^k + \phi_{j,i-1}^k}{\Delta z^2} + \frac{\phi_{j+1,i}^k - \phi_{j-1,i}^k}{2r_j \Delta r} = -\alpha n_j^k$$

where j is the index for the radial coordinate, i is the index for the z coordinate and the superscript k represents the index for the temporal coordinate t. We have reversed what would be considered the usual indexing, namely, i for the radial coordinate and j for the z one so as to minimize confusion with complex variables that will be introduced later, for stability analysis of equations that are purely radially dependent.

This may be rearranged giving

$$\phi_{j,i}^k = [(2r_j \Delta z^2 (\phi_{j+1,i}^k + \phi_{j-1,i}^k) + 2r_j \Delta r^2 (\phi_{j,i+1}^k + \phi_{j,i-1}^k) + \Delta r \Delta z^2 (\phi_{j+1,i}^k - \phi_{j-1,i}^k)$$
$$+ 2\alpha r_j \Delta r^2 \Delta z^2 n_j^k)][4r_j(\Delta r^2 + \Delta z^2)]^{-1}; \tag{3.7}$$

which is used only for the domain of the sample. From this we may then propagate the potential to the area of the chamber above and below the sample which must obey Laplace's equation (3.3). We use a central finite difference representation of the same form as (3.7) but putting a equal to zero; thus

$$\phi_{j,i}^k = \frac{(2r_j \Delta z^2 (\phi_{j+1,i}^k + \phi_{j-1,i}^k) + 2r_j \Delta r^2 (\phi_{j,i+1}^k + \phi_{j,i-1}^k) + \Delta r \Delta z^2 (\phi_{j+1,i}^k - \phi_{j-1,i}^k))}{4r_j(\Delta r^2 + \Delta z^2)}. \tag{3.8}$$

The remaining area for calculation is that of an annulus between the sample and the chamber, that is $R_s \leqslant r \leqslant R_c$ for $z = H_s$, as well as representations for (3.7) and (3.8) at $r = 0$. We now consider the latter.

For the annulus, a normal central difference scheme is that represented by (3.8); however, to propagate the potential radially from the sample a backwards scheme may be employed.

Thus the backwards finite radial representation of (3.3) with central z is

$$\frac{\phi_{j,i}^k - 2\phi_{j-1,i}^k + \phi_{j-2,i}^k}{\Delta r^2} + \frac{\phi_{j,i+1}^k - 2\phi_{j,i}^k + \phi_{j,i-1}^k}{\Delta z^2} + \frac{3\phi_{j,i}^k - 4\phi_{j-1,i}^k + \phi_{j-2,i}^k}{2r_j\Delta r} = 0;$$

which, after some algebra, can be solved:

$$\phi_{j,i}^k = \frac{(2r_j\Delta r^2(\phi_{j,i+1}^k + \phi_{j,i-1}^k) + 2r_j\Delta z^2(\phi_{j-2,i}^k - 2\phi_{j-1,i}^k) + \Delta r\Delta z^2(\phi_{j-2,i}^k - 4\phi_{j-1,i}^k))}{2r_j(\Delta z^2 - 2\Delta r^2) + 3\Delta r\Delta z^2}.$$

$$(3.9)$$

This may be used in conjunction with the purely central scheme of (3.8) to further guarantee that the gradient of the potential function across the radial boundary of the sample is continuous.

The above finite difference representations may be used to determine numerically the potential for the whole chamber generated from an initial charge carrier density, which for our case is taken as a constant. We have not included, however, the leftmost boundary of the plane—that is, that for $r = 0$—to which we now turn our attention.

Consider Poisson's equation (3.1):

$$\frac{1}{r}\frac{\partial}{\partial r}\left(r\frac{\partial\phi}{\partial r}\right) + \frac{\partial^2\phi}{\partial z^2} = -\alpha n(r, t). \tag{3.10}$$

In order to deal with $r = 0$ we need only consider the radial component of the Laplacian, namely

$$\frac{1}{r}\frac{\partial}{\partial r}\left(r\frac{\partial\phi}{\partial r}\right); \tag{3.11}$$

and if we now consider the Taylor series expansion of ϕ about $r = 0$ keeping z constant and taking ϕ as dependent only on r for the expansion we have

$$\phi(r) = \phi(0) + r\frac{\partial\phi(0)}{\partial r} + \frac{1}{2}r^2\frac{\partial^2\phi(0)}{\partial r^2} + \cdots; \tag{3.12}$$

however, due to the angular symmetry of our system, the gradient at $r = 0$ must be zero. Thus we have

$$\phi(r) = \phi(0) + \frac{1}{2}r^2\frac{\partial^2\phi(0)}{\partial r^2} + \cdots;$$

and therefore

$$\frac{1}{r}\frac{\partial}{\partial r}\left(r\frac{\partial\phi}{\partial r}\right) = \frac{1}{r}\frac{\partial}{\partial r}\left(r\frac{\partial\phi(0)}{\partial r} + r^2\frac{\partial^2\phi(0)}{\partial r^2} + \cdots\right) = 2\frac{\partial^2\phi(0)}{\partial r^2} + \cdots. \tag{3.13}$$

Now writing $\mathrm{d}r$ for r in (3.12) we have

$$\phi(\mathrm{d}r) - \phi(0) = \frac{1}{2}\mathrm{d}r^2\frac{\partial^2\phi(0)}{\partial r^2} + \cdots;$$

and so (3.13) may be written to second-order approximation as

$$\frac{1}{r}\frac{\partial}{\partial r}\left(r\frac{\partial\phi}{\partial r}\right) = \frac{4(\phi(\mathrm{d}r) - \phi(0))}{\Delta r^2} = \frac{4(\phi_1 - \phi_0)}{\Delta r^2}.$$

Thus if we now incorporate the z coordinate, we obtain the second-order finite difference equation for $r = 0$ as

$$\frac{4(\phi_{1,i}^k - \phi_{0,i}^k)}{\Delta r^2} + \frac{\phi_{0,i+1}^k - 2\phi_{0,i}^k + \phi_{0,i-1}^k}{\Delta z^2} = -an_0^k;$$

which may be solved:

$$\phi_{0,i}^k = \frac{(adr^2 n_0^k + 4\phi_{1,i}^k)\Delta z^2 + (\phi_{0,i+1}^k + \phi_{0,i-1}^k)\Delta r^2}{4\Delta z^2 + 2\Delta r^2}; \tag{3.14}$$

which is the finite difference equation for (3.1) at $r = 0$. The same relation may be derived for (3.3) by substituting $a = 0$, thus obtaining

$$\phi_{0,i}^k = \frac{4\phi_{1,j}^k \Delta z^2 + (\phi_{0,i+1}^k + \phi_{0,i-1}^k)\Delta r^2}{4\Delta z^2 + 2\Delta r^2}. \tag{3.15}$$

Hence we use (3.14) for the single point $r = 0$ on the sample and (3.15) for $r = 0$ everywhere else.

Once the potential is determined for the entire mesh/chamber, it may then be recalculated for the next time step in the charge decay by using the finite difference equation for (3.2), which is valid only for the domain of the sample.

Using a central spatial scheme and an explicit temporal scheme, (3.2) can be represented by

$$\frac{n_j^{k+1} - n_j^k}{\Delta t} = \beta \left(\frac{(n_{j+1}^k - n_{j-1}^k)(\phi_{j+1,H_s}^k - \phi_{j-1,H_s}^k)}{4\Delta r^2} - \alpha(n_j^k)^2 \right)$$

which may be solved for the carrier concentration:

$$n_j^{k+1} = \beta \Delta t \left(\frac{(n_{j+1}^k - n_{j-1}^k)(\phi_{j+1,H_s}^k - \phi_{j-1,H_s}^k)}{4\Delta r^2} - \alpha(n_j^k)^2 \right) + n_j^k. \tag{3.16}$$

This is the carrier charge density for the next time step, and may then be substituted into the finite difference equation for (3.1), to propagate the potential and then to carry on the transport process for subsequent time steps.

In order to make a comparison between this computational model and data obtained from the experimental technique described in section 2, we need now to model the decay of the total charge across the surface of the sample. To do this we need to integrate (3.16) over the surface area of the sample, in which we choose to employ the composite Simpson rule, namely:

$$Q(t) = 2\pi q \int_0^{R_s} n_v(r,t) r \, dr$$
$$= 2\pi q \left(\frac{\Delta r}{3} \right) (r_0 n_0^k + 4r_1 n_1^k + 2r_2 n_2^k + \cdots + 2r_{N-2} n_{N-2}^k + 4r_{N-1} n_{N-1}^k) \tag{3.17}$$

where $n_v(r,t)$ merely emphasizes that $n(r,t)$ is a volume carrier density.

We now discuss the convergence and stability criteria for this explicit scheme.

3.1. Stability analysis

The von Neumann stability analysis relevant here is dependent on determining the behaviour of the round-off errors, which for certain limits may be expressed via Fourier series [10, 11]. This method, however, is only of use for linear, constant coefficient equations. We therefore use a modified version of the von Neumann method as outlined in [10].

Let e_j^k be the round-off error terms and $\widehat{n}_j^k$ be the physically computed values determined via implementing (3.16). The actual solutions of (3.16) may be written as

$$n_j^k = \widehat{n}_j^k + e_j^k; \tag{3.18}$$

which from substitution into (16) yields

$$\widehat{n}_j^{k+1} + e_j^{k+1} = \beta\Delta t\left(\left(\frac{(\widehat{n}_{j+1}^k - \widehat{n}_{j-1}^k)}{2\Delta r^2} + \frac{(e_{j+1}^k - e_{j-1}^k)}{2\Delta r^2}\right)\phi_r - \alpha(\widehat{n}_j^k + e_j^k)^2\right) + \widehat{n}_j^k + e_j^k.$$

(3.19)

Since $\widehat{n}_j^k$ are assumed to solve (3.16) we may subtract (3.16) from (3.19) to obtain the difference equation for the round-off error terms, namely

$$e_j^{k+1} = \beta\Delta t\left(\frac{(e_{j+1}^k - e_{j-1}^k)}{2\Delta r}\phi_r - \alpha(\widehat{n}_j^k + e_j^k)^2 + \alpha(\widehat{n}_j^k)^2\right) + e_j^k.$$

(3.20)

If it is now assumed that the change in $\widehat{n}_j^k$ for a step in either k or j is small compared to the actual value of $\widehat{n}_j^k$ at those points, then

$$|\Delta\widehat{n}_j^k| \ll |\widehat{n}_j^k|;$$

(3.21)

and as a consequence $(e_{j+1}^k - e_{j-1}^k)/2\Delta r$ and $(\widehat{n}_{j+1}^k - \widehat{n}_{j-1}^k)/2\Delta r$ are both small and $O(e_j^k)$; hence we may approximate higher orders to zero; and expanding the terms in (3.20) and neglecting the higher order terms as stated we obtain

$$e_j^{k+1} = b\Delta t\left(\frac{(e_{j+1}^k - e_{j-1}^k)}{2\Delta r}\phi_r - \alpha\widehat{n}_j^k e_j^k\right) + e_j^k.$$

(3.22)

We now assume that the coefficients of the difference equations are so slowly varying that they can be considered constant in space and time, thus giving the independent solutions the form of an eigenmode expansion, where i here is taken to be $\sqrt{-1}$. Since this equation is independent of z and hence of its index, no confusion with the use of 'i' should arise. We have

$$e_j^k = \zeta^k e^{i\lambda j\Delta r}$$

(3.23)

which we then substitute into (3.22):

$$\zeta^{k+1}e^{i\lambda j\Delta r} = \beta\Delta t\left(\frac{\zeta^k e^{i\lambda j\Delta r}(e^{i\lambda\Delta r} - e^{-i\lambda\Delta r})}{2\Delta r}\phi_r - \alpha\widehat{n}_j^k\zeta^k e^{i\lambda j\Delta r}\right) + \zeta^k e^{i\lambda j\Delta r}.$$

(3.24)

Simplifying this equation we obtain

$$\zeta = i\beta\Delta t\frac{\sin(\lambda\Delta r)}{\Delta r}\phi_r - \alpha\beta\Delta t\widehat{n}_j^k + 1.$$

(3.25)

The stability criterion for the series in (3.24) to converge is

$$|\zeta|^2 = \beta^2\left(\frac{\Delta t}{\Delta r}\right)^2\phi_r^2\sin^2(\lambda\Delta r) + (1 - \alpha\beta\Delta t\widehat{n}_j^k)^2 \leqslant 1.$$

(3.26)

Consider the case where $\sin(\lambda\Delta r) = 0$; then we have the condition

$$\alpha^2\beta^2(\Delta t)^2(\widehat{n}_j^k)^2 - 2\alpha\beta\Delta t\widehat{n}_j^k \leqslant 0;$$

(3.27)

which implies

$$\widehat{n}_j^k \leqslant \frac{2}{\Delta t\alpha\beta};$$

(3.28)

this must hold for all eigenvalues and hence is absolute. We also consider the case $\sin(\lambda\Delta r) = 1$ for which

$$\beta^2\left(\frac{\Delta t}{\Delta r}\right)^2\phi_r^2 + \alpha^2\beta^2(\Delta t)^2(\widehat{n}_j^k)^2 \leqslant 2\alpha\beta\Delta t\widehat{n}_j^k$$

(3.29)

$$\beta^2 \left(\frac{\Delta t}{\Delta r} \right)^2 \phi_r^2 \leqslant 0.$$

This is impossible for our physical system. If equation (3.26) were to be further constrained such that

$$\widehat{n}_j^k \leqslant \frac{1}{\Delta t \alpha \beta}, \tag{3.30}$$

then it may be seen that the stability requirements of (3.26), and hence (3.27), are still satisfied; and looking more closely at the condition (3.27), letting $x \equiv \alpha \beta \Delta t \widehat{n}_j^k$ and differentiating, we also see that (3.30) provides the minimum of the inequality. Taking the largest possible value for $\widehat{n}_j^k$ governed by the condition proposed in (3.30), namely,

$$\widehat{n}_j^k = \frac{1}{\Delta t \alpha \beta},$$

and substituting this into (3.26) for $\sin(\lambda \Delta r) = 1$, provides the usable condition

$$\frac{\Delta t}{\Delta r} \leqslant \frac{1}{|\beta \phi_r|}. \tag{3.31}$$

These two cases account for all possibilities and hence we obtain the criterion for the step size ratio as well as a limit that the numerically calculated solution may take for convergence. The first of these conditions (3.30) is most useful for determining limits for initial values, whereas the second condition (3.31) provides a general criterion for determining the spatial numerical mesh size for both equations (3.1) and (3.2).

While such analysis is based on approximation (i.e., discarding higher order error terms etc), in general it is considered a 'good guide'. It should be noted, however, that there are cases in which systems will still not converge even after satisfying the von Neumann analysis [10].

It may be estimated, and in fact seen from numerical investigations, that for most calculations $\beta \sim 10^{-12}$ and that the gradient is usually greater than one and varies for different geometries (Cartesian versus cylindrical) by only a few orders; hence we are looking at a condition for the step size ratio being approximately

$$\frac{\Delta t}{\Delta r} \leqslant O(10^{12}). \tag{3.32}$$

It is reasonable to suggest that this condition is always met for logically defined spatial and temporal step sizes (at least for the calculations in this work). During charge decay from the surface region we may take

$$n_j^k \leqslant n_j^0 \qquad \forall k \neq 0;$$

and thus we need only concern ourselves with the refined condition of (3.30):

$$\widehat{n}_j^0 \leqslant \frac{1}{\Delta t \alpha \beta}. \tag{3.33}$$

The initial carrier density for all points across the sample is, however, assumed to be a constant c and hence (3.33) becomes

$$n_0 \leqslant \frac{1}{\Delta t \alpha \beta}$$

where $\widehat{n}_j^0 = n(r, 0) \equiv n_0$, basically fixing an upper bound on what initial value the constant carrier density can take. Noting, however, that $\beta \sim 10^{-12}$, and that again for most cases $\alpha \sim 10^9$, we may approximate the product to be

$$\alpha \beta \cong O(10^{-21});$$

and so assuming that for most calculations a step size of $\Delta t \leqslant 1$ is appropriate, we have an approximate upper bound for the initial carrier density:

$$c \leqslant O(10^{21}).$$

Initial calculations of the surface carrier density via the theory in section 3 and in the section on experimental results will show that such limits may be quickly reached. The methodology is now clear. Condition (3.33) determines the temporal step size governed via the initial carrier density that can be obtained from experimental data. Condition (3.31) then determines the allowed step size for the spatial coordinate r.

We may, however, obtain an asymptotic solution for comparative use in the region of very small t ($t \ll 1$), where we refer the reader to [9] for the details:

$$n_v = \frac{n_0}{\alpha\beta n_0 t + 1}.$$

In [9] we show that the infinite plane solution for the inviscid Burgers equation corresponds to these asymptotic solutions for our carrier diffusion model and hence the following is of direct relevance, as we will compare results from our asymptotic model to experimental values.

The carrier density in the surface region of thickness Δz can be given via the overall volume density as

$$n_s = n_v \Delta z. \tag{3.34}$$

The experimentally measured voltage from the electrometer may also be expressed as

$$V = \frac{Q}{C} = \frac{n_s q 2A}{C} = \frac{n_v q \Delta z A}{C} = \chi \Delta z n_v. \tag{3.35}$$

Here A is the area of the sample, Q the total charge, C the capacitance and $\chi \equiv qA/C$. Therefore we have

$$\frac{V}{\chi \Delta z} = \frac{n_0}{\alpha\beta n_0 t + 1} \qquad \text{where } n_0 = n_{v0}$$

as the carrier density at $t = 0$.

Inversion of this equation yields

$$\frac{1}{V} = \frac{\alpha\beta}{\chi \Delta z} t + \frac{1}{V_0}. \tag{3.36}$$

Here V_0 is the initial electrometer voltage at $t = 0$ (see also [7–9]). If we were to plot, as in (3.36), $1/V$ against t we should obtain a linear graph; thus the slope and intercept of the line are easily seen to be

$$\text{Slope} = m = \frac{\alpha\beta}{\chi \Delta z} = \frac{qDC}{\Delta z A \varepsilon \varepsilon_0 kT} \tag{3.37}$$

$$\text{Intercept} = Y = \frac{1}{V_0}. \tag{3.38}$$

Then we may obtain the diffusion coefficient from (3.37)

$$D = \frac{m \Delta z A \varepsilon \varepsilon_0 kT}{qC}; \tag{3.39}$$

and from equations (3.34) and (3.35) we may determine the initial surface carrier density as being

$$n_{s0} = \frac{V_0}{\chi} = \frac{1}{\chi Y}. \tag{3.40}$$

Using both the Einstein–Nernst equation

$$\sigma = \frac{nq^2 D}{kT}$$

(where q = carrier charge; D = carrier diffusion constant; T = temperature; k = Boltzmann's constant) and (3.37), we may obtain an expression for the slope in terms of the initial surface conductivity:

$$m = \frac{\sigma_{s0} C}{q n_{s0} \Delta z \varepsilon \varepsilon_0 2A}; \qquad (3.41)$$

and hence a measurement of initial surface conductivity may be obtained via rearrangement to give

$$\sigma_{s0} = \frac{m q n_{s0} \Delta z \varepsilon \varepsilon_0 A}{C}. \qquad (3.42)$$

Noting that the conductivity is the reciprocal of resistivity we then obtain an expression for the initial surface resistivity:

$$\rho_{s0} = \frac{1}{m n_{s0} \Delta z \varepsilon \varepsilon_0 \chi} \qquad (3.43)$$

and the initial volume resistivity:

$$\rho_{v0} = \frac{1}{m \varepsilon \varepsilon_0 V_0} \qquad (3.44)$$

where we have used expression (3.40). Thus what we have obtained from the graphing of the data is the volume resistivity for $t \ll 0$ that can be directly calculated from the graphs of experimental data (i.e., determining the slope m for initial values of t). Similarly, from knowing the slope of the graph, we may also determine the resistivity coefficient, which is a principal goal of this work.

4. Experimental results

Using the technique discussed above, resistivity measurements have been made for various materials covering a fairly broad range of insulators. Obtaining the initial voltage from the experimental decay curve, the initial surface carrier density is obtained via (3.40)

$$n_{s0} = V_0 C / qA = n(r, 0) \equiv n_0 \qquad (4.1)$$

which is then used in the numerical model with a diffusion coefficient D that is modified appropriately such that the theoretical curve fits the experimental data.

The numerical domain mirrored that of the dimensions of the experiment scaled down linearly so as to reduce the mesh size, thus reducing the amount of numerical calculation. The number of spatial points, however, was such as to give the numerical simulation enough granularity to converge correctly. The radial coordinate was defined on a grid [0, 140] where $r = 0$ represents the central axis of the chamber, which was assumed to pass directly through the centre of the sample, and $r = 140$ represents the radius of the chamber. The radius of the sample was taken to be $r = 28$, and grounded at $r = 29$.

The potential function obtained from the numerical solution may be seen in figures 4.1(a) and 4.1(b) with focus limited to the domain r for clarity. We note that its initial profile follows that of the carrier distribution across the sample as one would expect. We see that it then approaches parabolic-like curves to then return to similar 'flat' profiles for much later times $t \gg 1$ like those for $t \ll 1$. This is to be expected and indeed was assumed in previous sections when obtaining the asymptotic model for the decay.

The above potential decay curves may be compared with the carrier density decay as shown in figures 4.2(a) and 4.2(b) for glass and mica respectively.
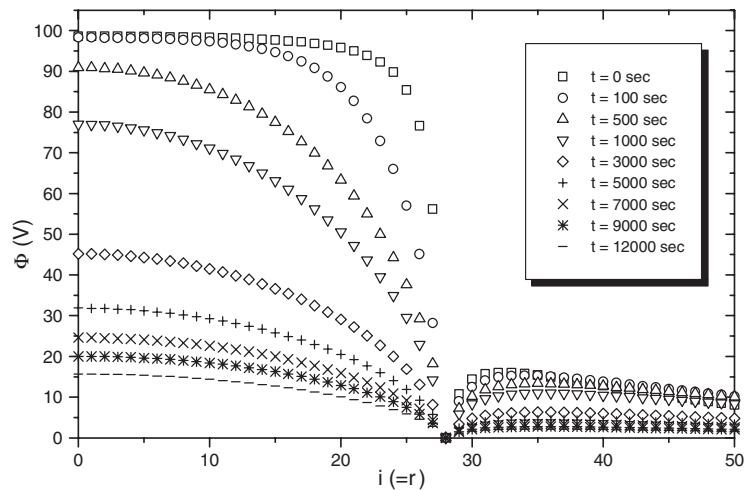
Figure 4.1. (a) The numerically derived potential function $\phi(r, H_s, t)$ decay for glass at various times.
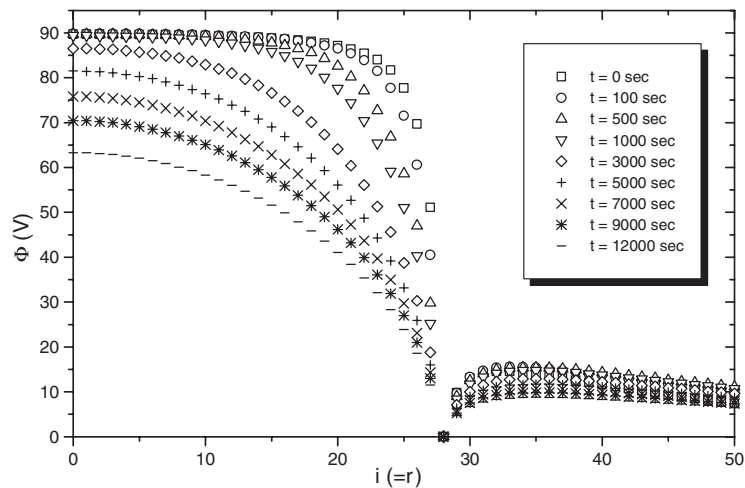

Figure 4.1. (b) The numerically derived potential function $\phi(r, H_s, t)$ decay for mica at various times.

4.1. Initial charge decay (experimental and theoretical comparison)

Asymptotic evaluation of resistivity. The charge transport theory and asymptotic results derived in sections 3 and 4 allow the measurement of the resistivity in the surface region of charged insulator samples from the observation of the initial phase of the charge decay. Plotting the reciprocal values of the voltage versus time for the early time period of the decay determines the resistivity in the surface region from equation (3.44). Figure 4.3 shows such plots for several insulator samples. The curves have been linearly least squares fitted.

From the slopes evaluated in figure 4.3 the resistivity for the material is then determined from equation (3.44) as shown in table 4.1. These resistivity values may be compared with
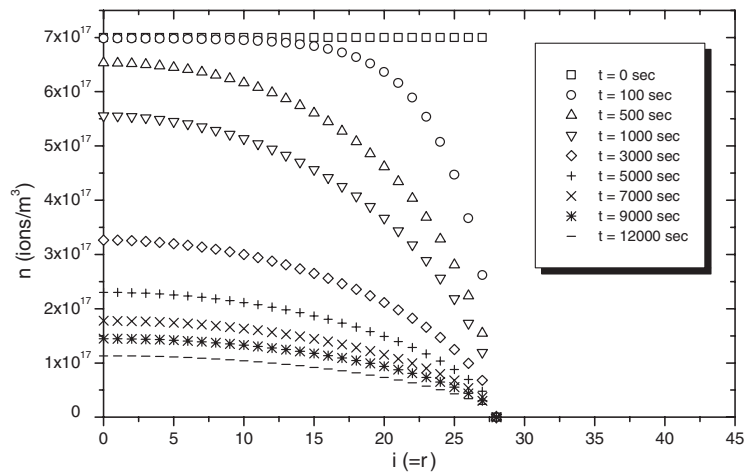
Figure 4.2. (a) The numerically derived carrier density $n(r, t)$ function decay on a glass disc, computed for the times indicated.
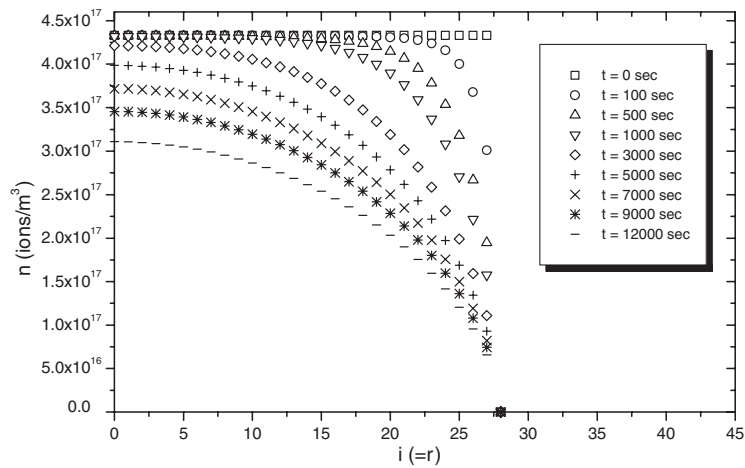

Figure 4.2. (b) The numerically derived carrier density $n(r, t)$ function decay on a mica disc, computed for the times indicated.

Table 4.1. Displaying the calculated slope of the linearly square fitted asymptotic profile, the correlation factor of the fit and the derived resistivity for the sample, via the use of the asymptotic formulae (3.44).

Sample	ε $\pm 6\%$	$1/V_0$	Slope	Correlation factor	ρ_{v0} (Ω m) $\pm 7\%$
Glass	5.00	0.50	1.4×10^{-3}	0.999	8.4×10^{12}
Perspex	3.40	0.34	4.4×10^{-4}	0.999	2.6×10^{13}
Mica	1.30	0.61	2.3×10^{-3}	0.999	2.3×10^{13}
Polyethylene	2.25	0.36	1.7×10^{-4}	0.991	1.1×10^{14}

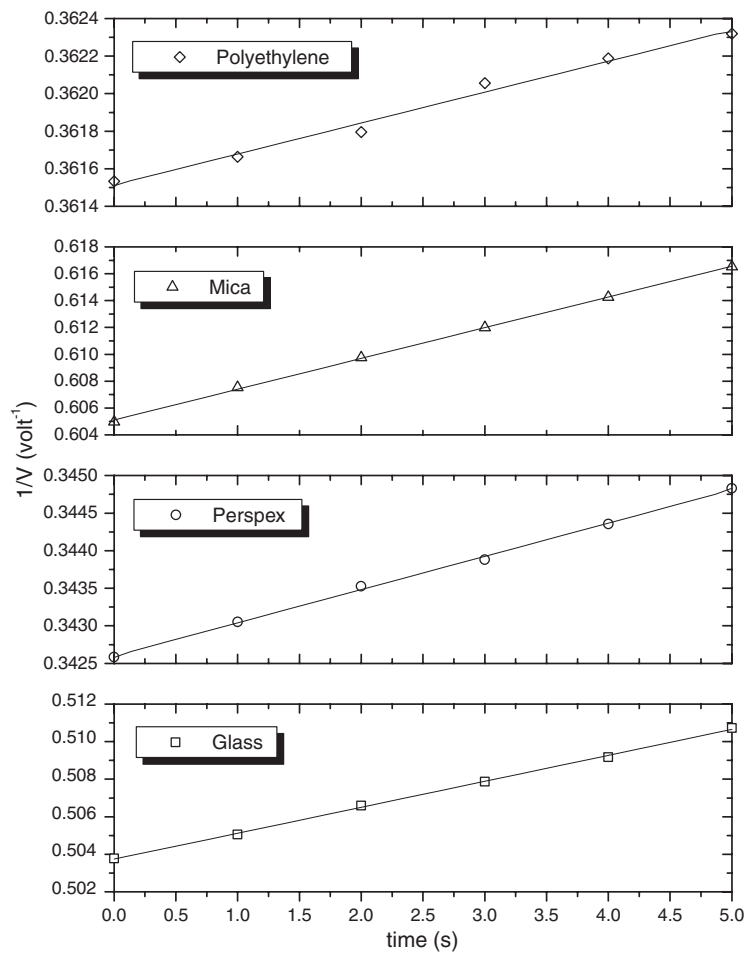the values obtained from the atmospheric measurement system in [5, 7, 8] and are shown in table 4.2.

Figure 4.3. (1/voltage) versus time plots for several insulators using data from the early time phase of charge decay.

Table 4.2. Displaying measured resistivity values for various samples using the atmospheric measurement system.

Sample	ε $\pm 6\%$	D (m^2 s^{-1}) $\pm 8\%$	ρ (Ω m) $\pm 7\%$	Reference
Glass	5.00	1.3×10^{-12}	2.3×10^{11}	[7]
Perspex	3.40	1.5×10^{-13}	6.7×10^{13}	[7]
Mica	1.30	6.6×10^{-13}	1.9×10^{12}	[5]
Polyethylene	2.25	6.5×10^{-18}	2.2×10^{16}	[7]

There is quite good agreement between the resistivity values obtained for the two methods, even though the values in table 4.1 are measured from initial charge decay data, whilst those in table 4.2 are not. This fact combined with the close agreement of the two results, indicates a higher accuracy in the refined vacuum method as compared to the atmospheric configuration, as would be expected.
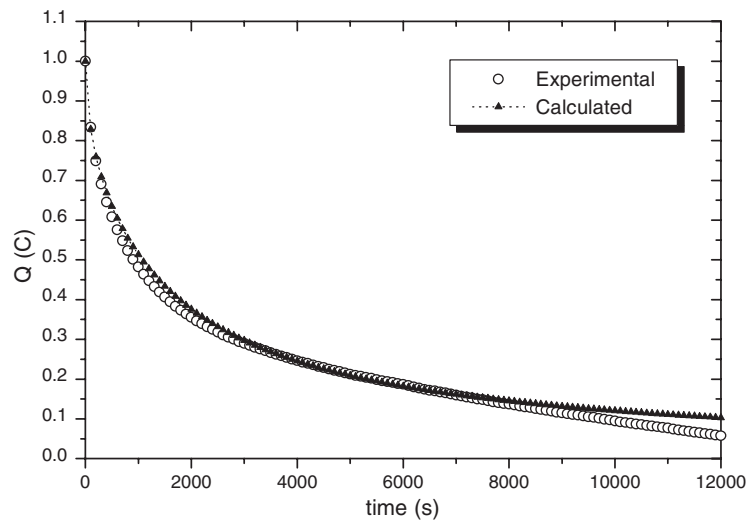
Figure 4.4. (a) Normalized theoretical and experimental charge decay versus time for glass; $(n_{v0} = 7 \times 10^{17}$ (ion m^{-3}), $D = 1.5 \times 10^{-12}$ (m^3 s^{-1}), $\Delta z = 3.4 \times 10^{-5}$ (m)).
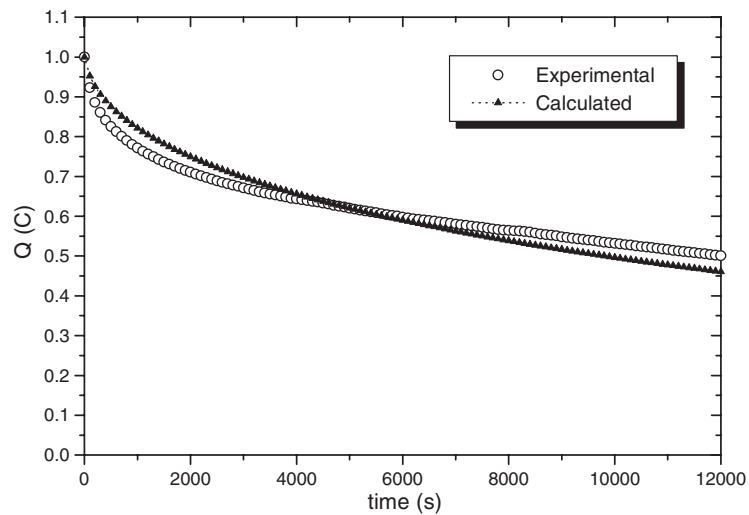

Figure 4.4. (b) Normalized theoretical and experimental charge decay versus time for Perspex; $(n_{v0} = 4.3 \times 10^{17}$ (ion m^{-3}), $D = 1.8 \times 10^{-13}$ (m^3 s^{-1}), $\Delta z = 8.1 \times 10^{-5}$ (m)).

4.2. Longer time charge decay (experimental and theoretical comparison)

Evaluation of diffusion coefficient, initial carrier density and surface charge depth.
Numerical integration of the charge density decay over time via the composite Simpson rule
in (3.17) provides a charge decay curve that may then be normalized and compared against
experimental data, as shown in figures 4.4(a)–4.4(d), for glass, Perspex, mica and polyethylene,
respectively.

From comparison of the theoretical (numerical) and experimental charge decay curves for
the entire decay spectrum, the initial surface charge density n_{s0} (ion m^{-2}), diffusion constant
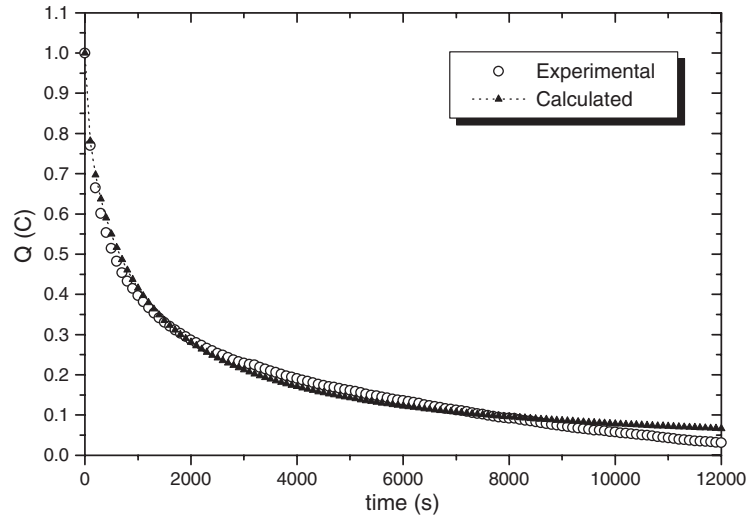
Figure 4.4. (c) Normalized theoretical and experimental charge decay versus time for mica; ($n_{v0} = 6.9 \times 10^{17}$ (ion m^{-3}), $D = 6.5 \times 10^{-13}$ (m^2 s^{-1}), $\Delta z = 2.9 \times 10^{-5}$ (m)).
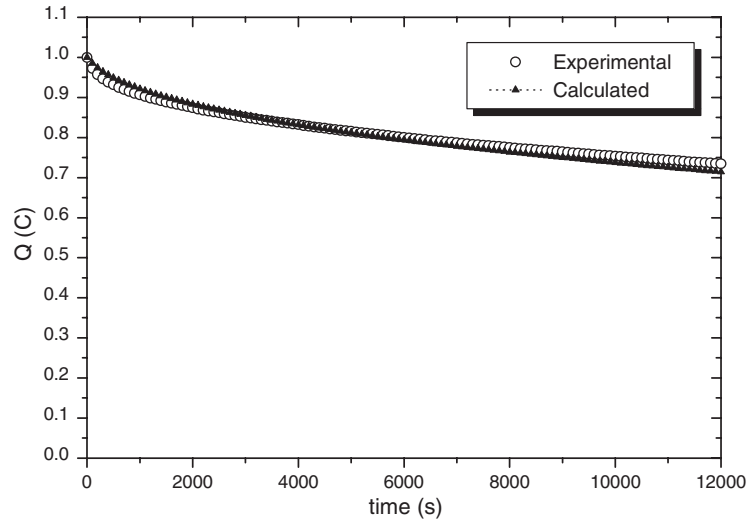

Figure 4.4. (d) Normalized theoretical and experimental charge decay versus time for polyethylene; ($n_{v0} = 3.4 \times 10^{21}$ (ion m^{-3}), $D = 6.5 \times 10^{-18}$ (m^3 s^{-1}), $\Delta z = 1 \times 10^{-8}$ (m)).

D (m^2 s^{-1}) and the depth of the mobile surface charge Δz (m), have been obtained for the different materials investigated. From these values the Einstein–Nernst equation in section 3 may then be used to evaluate the resistivity of the material, namely

$$\rho = \frac{kT}{n_{s0}q^2D}. \tag{4.2}$$

The results obtained from this analysis and calculations are shown in table 4.3 along with tabulated values for resistivity obtained from values tabulated in the literature, for additional comparison.

Table 4.3. Displaying the values derived in this paper: resistivity values ρ, carrier diffusion coefficients D, initial carrier densities n_{v0}, the surface charge depths Δz, relative permittivity values (taken from [8]) and values of the resistivity taken from their indicated respective references.

Sample	ε $\pm 6\%$	D (m^2 s^{-1}) $\pm 8\%$	Δz (m) $\pm 8\%$	n_{v0} (ion m^{-3}) $\pm 5\%$	ρ (Ω m) $\pm 6\%$	ρ (Ω m) Literature	Reference
Glass	5.00	1.5×10^{-12}	3.4×10^{-5}	7.0×10^{17}	1.6×10^{11}	10^9–10^{11}	[1]
						10^{11}	[12]
						10^{10}	[4]
						2×10^{11}	[13]
Perspex	3.40	1.8×10^{-13}	8.1×10^{-5}	4.3×10^{17}	2.1×10^{12}	10^{13}	[4]
Mica	1.30	6.5×10^{-13}	2.9×10^{-5}	6.9×10^{17}	3.6×10^{11}	10^{11}–10^{15}	[1]
						10^{13}	[2]
						9×10^{12}	[14]
						9×10^{13}	[15]
						10^{15}	[4]
Polyethylene	2.25	3.4×10^{-18}	1.0×10^{-8}	3.4×10^{21}	1.4×10^{13}	10^{13}–10^{16}	[1]
						10^{14}	[2]
						10^{18}	[3, 4]

Again we see good agreement with resistivity values from the previous atmospheric measurement system, as well as all results lying well within the range of tabulated literature values from the respective references. We note that the derived diffusion coefficient is significantly lower than that measured via the atmospheric technique. This may be attributed to moisture from the atmosphere aiding the conduction of carriers across the sample surface causing charge decay under atmospheric conditions to be faster than that in vacuum. This is reflected in the higher diffusion coefficient for the atmospheric measurements.

5. Conclusions

The incorporation of the methodology of Liesegang and Senn [5] for electrical resistivity measurement of insulators into a vacuum environment with new geometry has been successfully achieved. Reformulation of the transport equations for charge carriers in the surface regions of a disc-shaped sample and their numerical solution has allowed new measurements of resistivity for a range of common insulators. The vacuum environment will also permit future investigations to be carried out for surface modified samples, such as plasma treated surfaces. The derived values for the carrier diffusion constant and carrier depth have also been made available.

A new description of the transport physics, arrived at via a shock wave solution of the Burgers equation [9], has also allowed independent evaluation of the resistivity to be performed and resistivity estimates derived from predictions of that work have been usefully included in this work.

References

[1] Kaye G W C and Laby T H 1966 *Tables of Physical and Chemical Constants* (London: Longman)
[2] Van Vlack L H 1989 *Elements of Materials Science and Engineering* 6th edn (London: Addison-Wesley) (appendix C)
[3] Blyth A R 1980 *Electrical Properties of Polymers* (Cambridge: Cambridge University Press)

[4] Cross J A 1987 *Electrostatics: Principles, Problems, and Applications* (Bristol: Hilger)

[5] Liesegang J and Senn B C 1995 Resistivity of static and antistatic insulators from surface charge measurement *J. Appl. Phys.* **77** 5782 (erratum: the D values in table 1 of this paper are incorrect and should have read: Glass (2.0×10^{-12} m^2 s^{-1}); Mica (6.6×10^{-13} m^2 s^{-1}); Perspex (3.1×10^{-13} m^2 s^{-1}); Polyethylene (5.9×10^{-19} m^2 s^{-1}))

[6] *Annual Book of ASTM Standards, Standard Test Method for Electrostatic Charge* 1978 vol D2679-73 (New York: ANSI/ASTM)
    Standard Test Method for Static Electrification 1992 vol D4470-92 (New York: ASTM)

[7] Liesegang J and Senn B C 1996 Resistivity, charge diffusion and charge depth determinations on charged insulator surfaces *J. Appl. Phys.* **80** 6336

[8] Senn B C 1998 A surface resistivity study in insulators *Doctoral Thesis* La Trobe University Library, Melbourne VIC 3086, Australia

[9] Holcombe S R, Liesegang J and Smith E R 2004 Surface conductivity of insulators: 1-D initial value problems and the inviscid Burgers equation *J. Phys.: Condens. Matter* **16** 5999

[10] Street R L 1973 Numerical finite difference methods *The Analysis and Solution of Partial Differential Equations* (Pacific Grove, CA: Brooks/Cole) chapter 10

[11] Carnahan B, Lather H A and Wilkes J O 1969 *Applied Numerical Methods* (New York: Wiley)

[12] Callister W D Jr 2000 *Materials Science and Engineering* 5th edn (New York: Wiley)

[13] Bleaney B L and Bleaney B 1969 *Electricity and Magnetism* (Oxford: Oxford University Press)

[14] Duckworth H E 1960 *Electricity and Magnetism* (New York: Holt, Rinehart, and Winston)

[15] Ruoff A L 1973 *Materials Science* (Englewood Cliffs, NJ: Prentice-Hall) p 67